JOURNAL OF Materials CHEMISTRY

Crystal structure, physical properties and electronic structure of a new organic conductor β″-(BEDT-TTF)$_2$SF$_5$CHFCF$_2$SO$_3$†

John A. Schlueter,*[a] Brian H. Ward,[a] Urs Geiser,[a] Hau H. Wang,[a] Aravinda M. Kini,[a] James Parakka,[a] Emilio Morales,[a] H.-J. Koo,[b] M.-H. Whangbo,[b] R. W. Winter,[c] J. Mohtasham[c] and Gary L. Gard[c]

[a]*Materials Science Division, Argonne National Laboratory, Argonne IL 60439. E-mail: JASchlueter@anl.gov*
[b]*Department of Chemistry, North Carolina State University, Raleigh, USA NC 27695-8204*
[c]*Department of Chemistry, Portland State University, Portland, USA OR 97207-0751*

Received 30th October 2000, Accepted 30th April 2001
First published as an Advance Article on the web 14th June 2001

A new organic conductor, β″-(BEDT-TTF)$_2$SF$_5$CHFCF$_2$SO$_3$ [BEDT-TTF, hereafter abbreviated ET, refers to bis(ethylenedithio)tetrathiafulvalene], was prepared by electrocrystallization. The crystal structure of this salt was determined by single crystal X-ray diffraction at 298 and 150 K, its physical properties were examined by electrical resistivity, Raman spectroscopy and EPR measurements, and its electronic structure was calculated and compared with that of the analogous salt β″-(ET)$_2$SF$_5$CH$_2$CF$_2$SO$_3$. Whereas β″-(ET)$_2$SF$_5$CHFCF$_2$SO$_3$ has disordered anions and undergoes a metal-to-insulator transition at ~190 K, β″-(ET)$_2$SF$_5$CH$_2$CF$_2$SO$_3$ has ordered anions and is semiconducting down to ~100 K, metallic below ~100 K, and superconducting below 5 K. At room temperature both β″-(ET)$_2$SF$_5$CHFCF$_2$SO$_3$ and β″-(ET)$_2$SF$_5$CH$_2$CF$_2$SO$_3$ have similar electronic band structures and physical properties. When the temperature is lowered, each donor molecule stack becomes dimerized in both salts. However, the interdimer interaction within each donor stack nearly vanishes in β″-(ET)$_2$SF$_5$CHFCF$_2$SO$_3$, but remains substantial in β″-(ET)$_2$SF$_5$CH$_2$CF$_2$SO$_3$.

1. Introduction

Numerous organic superconductors have been found among the 2:1 salts of the electron-donor molecule BEDT-TTF [BEDT-TTF, hereafter abbreviated ET, refers to bis(ethylenedithio)tetrathiafulvalene].[1] These salts have a crystal structure in which layers of ET molecules are separated by layers of monovalent anions X^-. For these molecular crystals, a small modification in the anion structure induces a change in the packing motif of the donor molecule layer, the interactions between nearest-neighbor donor molecules, and hence a profound change in the physical properties. For example, the β-(ET)$_2$X salts with linear triatomic anions $X^- = I_3^-$, IBr_2^- and AuI_2^- are superconductors, with the highest T_c obtained for the largest (I_3^-) anion.[2–4] With shorter linear anions $X^- = ICl_2^-$ and $AuCl_2^-$, ET molecules form the β′-(ET)$_2$X salts that are magnetic semiconductors and undergo a three-dimensional antiferromagnetic phase transition at low temperatures.[5–7] Likewise, striking changes in physical properties are observed for the κ-(ET)$_2$Cu[N(CN)$_2$]X (X = Cl, Br, I) salts when the Cu–X bond length of the anion is gradually increased: κ-(ET)$_2$Cu[N(CN)$_2$]Cl is a semiconductor at ambient pressure, but becomes a superconductor under pressure (0.3 kbar, T_c = 12.8 K),[8] κ-(ET)$_2$Cu[N(CN)$_2$]Br is an ambient-pressure superconductor (T_c = 11.6 K),[9] but κ-(ET)$_2$Cu[N(CN)$_2$]I is not a superconductor.[10]

Recently, we reported a new ambient pressure organic superconductor, β″-(ET)$_2$SF$_5$CH$_2$CF$_2$SO$_3$ (T_c = 5.2 K, hereafter referred to as compound **I**).[11,12] We attempted to prepare an analogous superconductor by synthesizing the slightly larger $SF_5CHFCF_2SO_3^-$ anion (racemate) and carrying out electrocrystallization with ET. It was hoped that use of a larger anion with essentially identical shape would result in an isostructural superconductor with higher T_c. Instead, this work resulted in a new β″-type salt, β″-(ET)$_2$SF$_5$CHFCF$_2$SO$_3$ (hereafter referred to as compound **II**) which undergoes a metal-to-insulator (MI) transition below ~190 K, in sharp contrast to the case of **I**. Although the $SF_5CHFCF_2SO_3^-$ anion is chiral, this cannot be the sole reason for the destruction of the superconducting state because superconductivity is observed in β″-(ET)$_4$[(H$_3$O)Fe(C$_2$O$_4$)$_3$]·C$_6$H$_5$CN, which also possesses chiral anions in a racemic mixture.[13] In the present work, we describe the synthesis of **II** and characterize its crystal structure and physical properties. Then we probe why the transport properties of the **I** and **II** are so different by comparing their electronic structures based on the crystal structures determined at room temperature as well as at a temperature below the MI transition of **II**.

2. Experimental

ET was prepared as previously described[14,15] and recrystallized from chloroform (Aldrich) prior to use. $SF_5CHFCF_2SO_3Na$ was prepared as previously described.[16] 18-Crown-6 (Aldrich) was recrystallized from dry acetonitrile prior to use.[17] 1,1,2-Trichloroethane (TCE, Fluka) was distilled from P_2O_5 (Aldrich) and filtered through a column containing neutral alumina prior to use. Tetrahydrofuran (THF) was distilled from sodium–benzophenone prior to use. Dichloromethane (Aldrich, 99.9%, A.C.S. HPLC grade) and chlorobenzene (Aldrich, 99.6%, A.C.S. reagent) were used without further purification.

Short black rod-like crystals of **II** were grown by using the

†© U.S. Government. The submitted manuscript has been authored by a contractor of the U.S. Government under contract No. W-31-109-ENG-38. Accordingly, the U.S. Government retains a nonexclusive, royalty-free license to publish or reproduce the published form of this contribution, or allow others to do so for U.S. Government purposes.

 DOI: 10.1039/b008735l

This journal is © The Royal Society of Chemistry 2001

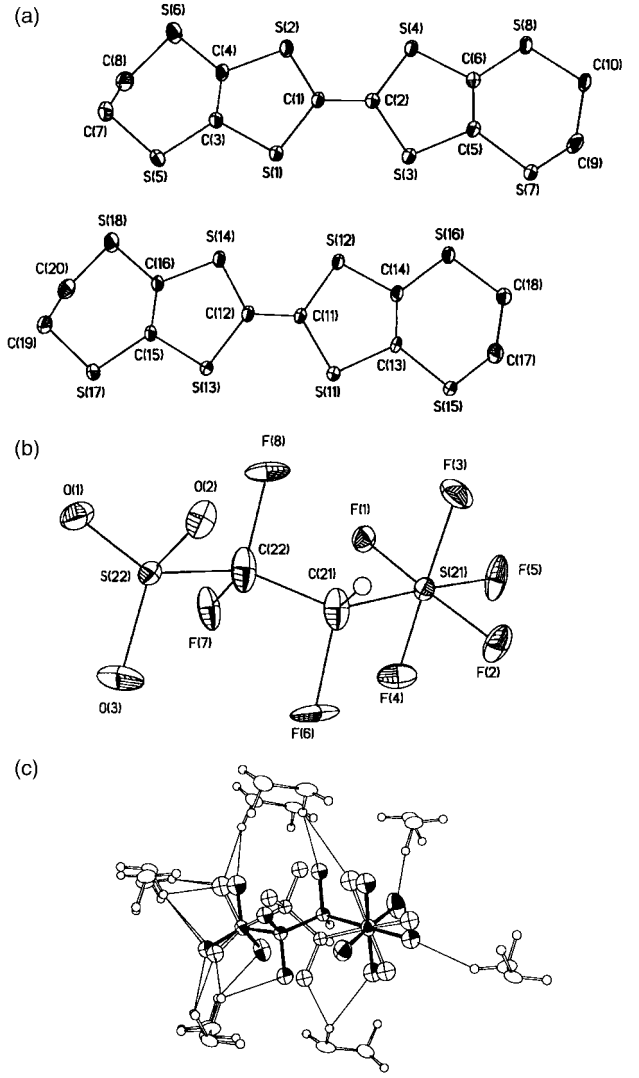

Fig. 1 (a) Atom numbering used for the donor molecules of **II**. Hydrogen atoms have been omitted for clarity. (b) Atom numbering used for the anions of **II**. Only the majority conformation is shown for clarity. (c) The disordered anion pocket of **II**, illustrating the many short intermolecular contacts between the hydrogen atoms of ET and the electronegative oxygen and fluorine atoms of the $SF_5CHFCF_2SO_3^-$ anion.

previously described electrocrystallization techniques.[18,19] The electrochemical cell was assembled in an argon filled dry box. Excess $SF_5CHFCF_2SO_3Na$ and 18-crown-6 were added to both chambers of an H-cell. ET (8.3 mg, 0.022 mmol) was loaded into the anode chamber. The crystallization solvent, dichloromethane (7.5 ml), was then added to each chamber of the H-cell. A current density of 0.19 μA cm^{-2} was initially applied and gradually increased over a period of six days to 0.75 μA cm^{-2}, at which time crystallization of black crystals commenced on the electrode surface and the cell walls. Crystals were grown at 25 °C on platinum wire electrodes for a period of 20 days. The best crystals of **II** grew when dichloromethane or 1,1,2-trichloroethane was used as the solvent. Poor quality crystals were obtained when tetrahydrofuran or chlorobenzene was the crystallization solvent.

The carbon atom of the $SF_5CHFCF_2SO_3^-$ anion is stereogenic, and the synthetic procedure leading to this anion results in a racemic mixture of the *R*- and *S*-configurations of the anion. This racemic mixture was used for the electrocrystallization of **II** by employing the electrocrystallization techniques as previously described. Single crystal X-ray crystallography indicates that both configurations of the $SF_5CHFCF_2SO_3^-$ anion are equally incorporated into the crystal lattice. Attempts to separate the $SF_5CHFCF_2SO_3^-$ enantiomers through preparation of a brucine salt were unsuccessful.

The single crystal structures of **II** were determined at 298 and 150 K by X-ray diffraction using a Siemens SMART® single crystal X-ray diffractometer equipped with a CCD-based area detector and a sealed-tube X-ray source. Further details are available in a .cif file deposited as electronic supplementary information (ESI). EPR measurements were performed on an IBM ER-200 X-band spectrometer equipped with a TE_{102} microwave cavity and an Oxford EPR-900 flow cryostat with an ITC4 temperature controller. The temperature dependence of the electrical resistivity of **II** was measured by using the conventional four-probe DC technique with a LakeShore Model 7000 cryostat equipped with RES7000 software. Four gold contacts (~3000 Å thick) in a linear arrangement were made on a single rod-like crystal sample (4.0 mm × 0.32 mm × 0.32 mm) of **II** by thermal evaporation, and narrow gauge (0.0005 inch diameter) gold wires were affixed to the contacts using fast drying silver paint. Resistivity data were recorded during both the cooling and warming cycles with a slow cooling/warming rate of about 1 °C min^{-1} utilized to prevent microcracking of either the crystal or contacts. A DC current of 1.0 mA was applied. Raman spectra were recorded using a Raman microscope spectrometer (Renishaw, Ltd.) equipped with a He : Ne ($\lambda_o = 6328$ Å) laser. A low laser power of 0.06 mW focused on a 1 μm^2 area was applied. The spectra were averaged over 20 scans. Raman shifts between 50 and 2500 cm^{-1} were recorded and calibrated against the standard Si peak at 520 cm^{-1}.

3. Crystal structures

Figs. 1a and 1b show the atom numbering used for the donor molecules and the anions of **II**. Table 1 summarizes the crystallographic data for **II** at 298 K and 150 K. For comparison, this Table also lists the crystallographic data for **I** at 298 and 123 K.

As in most salts of ET, the structures of **I** and **II** are characterized by layers of donor molecules separated by layers of anions. The ET molecules in these salts are arranged in tilted stacks along the *a*-axis. Both of these salts contain two crystallographically nonequivalent ET molecules (denoted A and B). As depicted in Fig. 2 for the room temperature structure of **II**, each donor stack consists of only one type (A or B) of donor molecule, and stacks of molecules A alternate with stacks of molecules B. Donor molecules A and B in adjacent

Table 1 Summary of crystallographic data for β″-$(ET)_2SF_5CH_2CF_2SO_3$ (**I**) and β″-$(ET)_2SF_5CHFCF_2SO_3$ (**II**)

Compound	**I**		**II**	
Reference	11		This work	
Chemical formula	$C_{22}H_{18}F_7O_3S_{18}$		$C_{22}H_{17}F_8O_3S_{18}$	
FW/g mol^{-1}	1040.45		1058.44	
a/Å	9.260(2)	9.1536(6)	9.2233(5)	9.2462(4)
b/Å	11.635(2)	11.4395(8)	11.5932(6)	11.3610(5)
c/Å	17.572(5)	17.4905(12)	17.8088(9)	17.7145(8)
α/deg	94.69(3)	94.316(1)	93.863(1)	94.121(1)
β/deg	91.70(1)	91.129(1)	94.543(1)	94.914(1)
γ/deg	103.10(2)	102.764(1)	103.071(1)	103.139(1)
V/$Å^3$	1835.5(9)	1779.9(2)	1841.9(2)	1797.45(13)
Z	2	2	2	2
Space group	$P\bar{1}$	$P\bar{1}$	$P\bar{1}$	$P\bar{1}$
Temperature/K	298	123	298	150
λ/Å			0.71073	0.71073
ρ_{calcd}/g cm^{-3}			1.908	1.953
μ/mm^{-1}			1.12	1.15
$R(F_o)$ $(I > 2\sigma)^a$			0.079	0.053
$R_w(F_o)^a$			0.074	0.057

$^a R(F_o) = \sum||F_o| - |F_c||/\sum|F_o|$, $R_w(F_o) = [\sum w(F_o^2 - F_c^2)^2/\sum wF_o^4]^{1/2}$

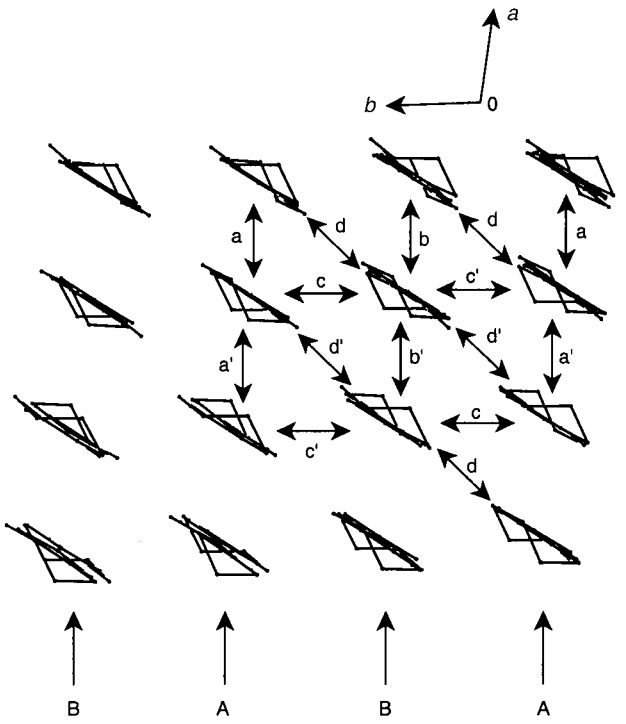

Fig. 2 Packing pattern of the ET molecules in the donor layer of **II**, where the labels between adjacent ET molecules define the nearest-neighbors i and j for the HOMO–HOMO interaction energies β_{ij} listed in Table 2.

stacks form nearly coplanar arrays along the $(a+b)$ direction. The short S···S intermolecular contacts are primarily between molecules on adjacent stacks.

The ethylene end-groups of the ET molecules in **I** are ordered in an eclipsed conformation at 123 K. In contrast, all the ethylene groups in the structure of **II** are disordered at room temperature, but order in a staggered conformation at 150 K.

The charge of the ET molecules in the low temperature structures of **I** and **II** has been determined through an analysis of the C–S and C=C bond lengths as described by Guionneau *et al.*[20] At 150 K, the two independent ET molecules in **II** were found to have charges of +0.60 and +0.49. Normalizing the sum of these charges to +1, the charges on the ET molecules are scaled to +0.55 and +0.45. A similar analysis for **I** yields charges of +0.62 and +0.47, which scale to +0.57 and +0.43.

As illustrated in Fig. 1c, the $SF_5CHFCF_2SO_3^-$ anion is disordered in the structure of **II**. This is due to a competition for hydrogen bonding between the hydrogen atoms of the ET electron-donor molecules and the electronegative fluorine atoms of the anion. In contrast, in **I**, there are no short H···F contacts between the CF_2 fluorine atoms of the $SF_5CH_2CF_2SO_3^-$ anion and the hydrogen atoms of ET. As a result, **I** contains an ordered anion. It should be noted that the presence of a racemic mixture does not require crystallographic disorder, as the anion is on a general position in the centrosymmetric space group, and each enantiomer will be represented once in the unit cell.

CCDC reference number 158389, 158390. See http://www.rsc.org/suppdata/jm/b0/b008735l/ for crystallographic files in .cif format.

4. Physical properties

The electrical resistivity data of **II** measured as a function of temperature are presented in Fig. 3. This salt is metallic down to ~190 K, below which it undergoes an MI transition. In addition, the resistivity curves for the cooling and warming cycles show a strong hysteresis. We previously reported the

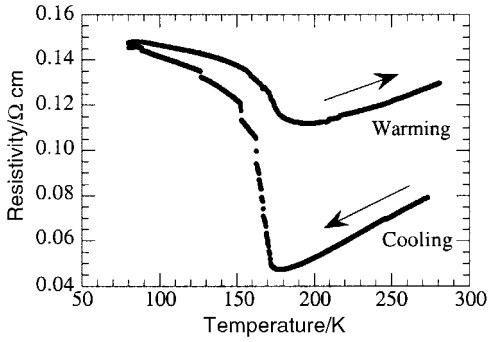

Fig. 3 Temperature dependence of the electrical resistivity measured for single crystals of **II**.

variable temperature resistivity data of **I**.[11,12] This salt shows weakly semiconducting behavior down to ~100 K, below which it becomes metallic and eventually superconducting below 5.2 K.[11]

Variable temperature EPR studies carried out for compound **II** are summarized in Fig. 4. The ambient temperature EPR line width of 35 G is similar to that which we previously reported for **I**[11] and typical of ET salts with a β″-type structure. The spin susceptibility remains nearly constant above ~180 K and decreases sharply between ~180 and ~100 K. With decreasing the temperature further, the susceptibility decreases slowly and becomes almost negligible. The temperature-independent spin susceptibility above 180 K is consistent with a metallic character, and the susceptibility decrease with decreasing temperature in the 180–100 K region indicates a thermal activation process associated with an energy gap. These observations are consistent with the results of the electrical resistivity measurements discussed above.

Recently, we extracted the anisotropic microwave conductivities of **I** by analyzing the Dysonian derivative line shapes of its EPR spectrum.[12] At room temperature this study examined how the microwave conductivity of the donor molecule plane depends on the orientation of the donor layer with respect to the magnetic field by analyzing the orientational dependence of the line width ΔH and g-value. To carry out a similar analysis for **II**, we measured the orientation dependence of the ΔH and g values. For this experiment, the crystal was rotated around the c^*-axis with 0° indicating that the static magnetic field was perpendicular to the long crystal axis (*i.e.*, along the b-axis). Under these conditions, the microwave electric field was always parallel to the highly conductive ab-plane, and the EPR spectra were Dysonian in line shape. The data are summarized in Fig. 5a. The analysis of these data leads to the microwave conductivities plotted in Fig. 5b, which shows that the conductivity is highest along the direction of $\theta = 100°$. This coincides with the crystallographic b-axis (*i.e.*, interstack) direction, as also found for **I**.[12]

The ambient temperature Raman spectra of **I** and **II** are

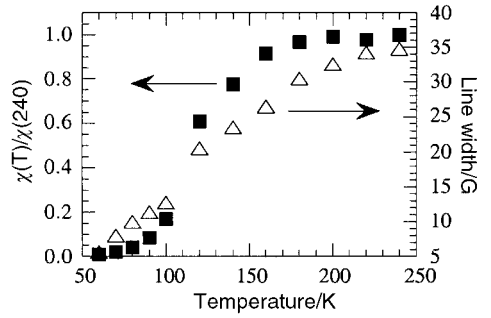

Fig. 4 Line widths (open triangles) and relative spin susceptibility (filled squares) of **II** as a function of temperature.

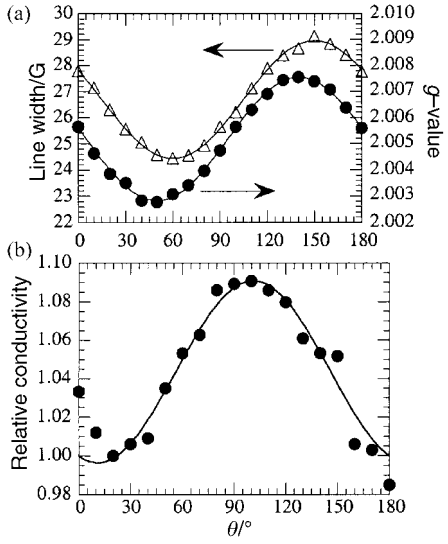

Fig. 5 (a) Line widths (G) and *g*-values of **II** as a function of rotation around the crystallographic *c**-axis. (b) *ab*-plane microwave conductivity (derived from the data of Fig. 5a) as a function of rotation around the crystallographic *c**-axis.

shown in Fig. 6, which highlights only the v_3 (A_g) mode that involves the stretching vibration of the central C=C double bond of ET.[21,22] The two salts have a peak corresponding to the v_3 mode at 1470 cm^{-1}. Since this peak is not split, all ET molecules are practically equivalent in both **I** and **II**, although each salt has two crystallographically nonequivalent ET molecules. Based on the Raman data, the ET molecules have an oxidation state of about +0.5 at room temperature.

The room temperature optical conductivity of **I** shows optical transitions in the energy region of 0–0.75 eV,[23–25] which are found to be intraband transitions associated with the bands that result from the highest-occupied molecular orbitals (HOMO's) of the ET molecules.[25] The optical conductivity is much stronger along the interstack direction (*b*-axis direction) than along the direction perpendicular to it throughout the energy region of 0–0.75 eV. This anisotropy is explained by the fact that the HOMO bands are more strongly dispersive along the interstack than along the intrastack direction.[25] Compound **II** exhibits room temperature optical excitations quite similar to those found for **I** in the 0–0.75 eV region, and additional excitations around 1 eV not found for **I**.[24] At present the origin of these additional excitations in **II** is not clear.

5. Electronic structure of β″-$(ET)_2SF_5CHFCF_2SO_3$

The electronic structure of **II** was examined by performing electronic band structure calculations based on the extended Hückel tight binding (EHTB) method.[26,27] Fig. 7a shows the dispersion relations calculated for the highest four occupied bands of **II** at room temperature. The highest two occupied

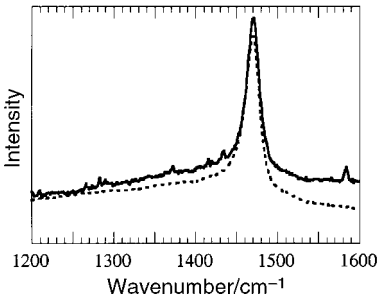

Fig. 6 Raman spectra measured for single crystals of **I** (solid line) and **II** (dashed line).

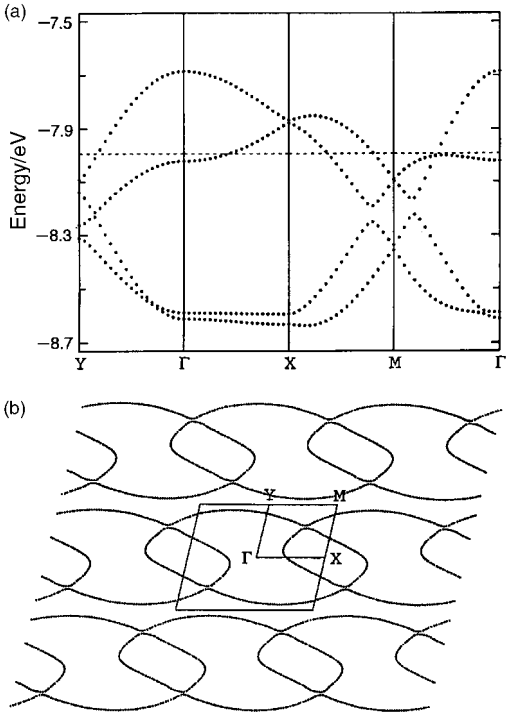

Fig. 7 (a) Dispersion relations of the four highest occupied bands calculated for **II** at room temperature, where the dashed line refers to the Fermi level, Γ = (0, 0), X = (*a**/2, 0), Y = (0, *b**/2) and M = (*a**/2, *b**/2). (b) Fermi surfaces associated with the partially filled bands of Fig. 7a in an extended zone.

bands are partially filled, and the Fermi surfaces associated with these bands are shown in Fig. 7b. Within the first primitive zone, the Fermi surfaces consist of a closed hole pocket centered at X and a pair of wavy lines straddling the M→Y line. Namely, **II** has both one-dimensional (1D) and two-dimensional (2D) Fermi surfaces, and these features are entirely analogous to those found for **I**.[12,28]

To a first approximation, the 2D hole pocket predicts an isotropic conductivity in the plane of the donor layer. A metal with a 1D surface composed of parallel lines has a maximum conductivity along the direction perpendicular to the lines, and a minimum conductivity along the direction parallel to the lines. Thus the 1D Fermi surface of Fig. 7b predicts the maximum conductivity along the *b*-axis direction (*i.e.*, perpendicular to M→Y), and the minimum conductivity along Γ→X (*i.e.*, along the stacking direction), in good agreement with the observed anisotropy in the *ab*-plane microwave conductivity (Fig. 5b).

6. Differences in the electronic structures of β″-$(ET)_2SF_5CHFCF_2SO_3$ and β″-$(ET)_2SF_5CH_2CF_2SO_3$

As described above, the electronic band structure of **II** is similar to that of **I** at room temperature. Nevertheless, the two salts are quite different in the temperature dependence of their electrical resistivities. To help understand why the two salts are so different, we examine how strongly nearest-neighbor ET molecules interact in their donor layers by calculating the HOMO–HOMO interaction energies $\beta_{ij} = <\psi_i|H^{eff}|\psi_j>$,[29] where H^{eff} is an effective Hamiltonian, and ψ_i and ψ_j are the HOMO's of nearest-neighbor ET molecules i and j, respectively. Table 2 summarizes the β_{ij} values calculated for the two salts, which show that at room temperature, compounds **I** and **II** are similar. Namely, the stack of molecules A has a stronger dimerization than does the stack of molecules B, and the interstack interactions are very similar. As the temperature is

Table 2 HOMO–HOMO interaction energies β_{ij} (in meV) between the nearest-neighbor BEDT-TTF molecules in the donor molecule layers of β″-$(ET)_2X$ (**I**: $X = SF_5CH_2CF_2SO_3^-$, **II**: $X = SF_5CHFCF_2SO_3^-$)

	I		**II**	
ij pair	298 K	123 K	298 K	150 K
Intrastack				
a	106	116	273	133
a′	25	58	72	8
b	69	124	33	127
b′	63	55	64	1
Interstack				
c	260	259	274	289
c′	275	271	266	291
d	118	138	137	149
d′	130	154	106	72

lowered to 150 K in **II**, the dimerization in the molecule A stack is weakened while a strong dimerization takes place in the molecules B stack. As a result, the degree of dimerization in both stacks becomes equal, and the interaction between dimers practically vanishes within each donor stack. The latter is conducive for electron localization (see below for further discussion). When the temperature is decreased to 123 K in **I**, the dimerization in the molecule A stack is weakened, and a strong dimerization takes place in the molecules B stack, such that the degree of dimerization in both stacks becomes equal. These findings are similar to those found for **II**. However, the interaction between adjacent dimers within each donor stack of **I** remains substantial, which is conducive to electron delocalization.

Let us now consider a probable electron localization for **II** below ~180 K. From the fact that each donor stack is strongly dimerized, one might suppose that an unpaired spin occurs in each donor dimer. This would result in a high spin susceptibility, but Fig. 4 shows that the spin susceptibility decreases sharply below ~180 K and becomes negligible below ~100 K, thus implying the pairing up of spins. It is noted from Table 2 that the β_{ij} values between adjacent dimers along the interstack direction are substantial in **II** at the low temperature. In other words, the donor layer of **II** contains chains of dimers running along the interstack direction, and hence this salt becomes a 1D metal with a half-filled band dispersive along the interstack direction. The spin susceptibility would diminish as observed from the EPR measurements, if a pairing distortion takes place along the interstack direction. To test this hypothesis, it will be necessary to determine the crystal structure of **II** at a low temperature well below ~150 K.

It should be recalled that the conformations of the anions and the donor molecule ethylene groups are disordered in **II**, but this is not the case in **I**. We speculate that the hysteresis in the electrical resistivity of **II** implies that the positions of the anions and the ethylene groups undergo relaxation. Such a relaxation would depend on whether the sample is being cooled or warmed thereby changing the mobility of the charge carriers differently. Future NMR studies are planned to this effect.

7. Concluding remarks

The $SF_5CHFCF_2SO_3^-$ and $SF_5CH_2CF_2SO_3^-$ anions are similar in shape and size. Likewise, the two salts **I** and **II** are similar in both their crystal and electronic structures. Nevertheless, the transport properties of the two salts are strikingly different. Compound **II** undergoes an MI transition at ~190 K, and its electrical resistivity is strongly hysteretic. In contrast, **I** is semiconducting down to ~100 K, below which it is metallic and becomes superconducting below 5.2 K. As the temperature is lowered, each donor stack of the donor layers becomes dimerized in both salts. The interdimer interaction within each donor stack nearly vanishes in **II**, but remains substantial in **I**. This is probably why electron localization takes place in **II**. Our EPR spin susceptibility data for **II** suggest that a pairing distortion is likely to occur along the interstack direction. Due to the similarity in the crystal structures of the two salts, it should be possible to prepare crystal samples β″-$(ET)_2(SF_5CH_2CF_2SO_3)_x(SF_5CHFCF_2SO_3)_{1-x}$ in which we expect to see a dopant threshold at which the superconducting state disappears.

Acknowledgements

Work at Argonne National Laboratory is sponsored by the U.S. Department of Energy, Office of Basic Energy Sciences, Division of Materials Sciences, under Contract W-31-109-ENG-38. EM is a student undergraduate research participant, sponsored by the Argonne Division of Educational Programs, from Oberlin College, Oberlin, OH. Work at North Carolina State University is supported by the U.S. Department of Energy, Office of Basic Sciences, Division of Materials Sciences, under Grant DE-FG05-86ER45259. Work at Portland State University is supported by NSF grant No. CHE-9904316 and the Petroleum Research Fund ACS-PRF 34624-AC7.

References

1 J. M. Williams, J. R. Ferraro, R. J. Thorn, K. D. Carlson, U. Geiser, H. H. Wang, A. M. Kini and M. H. Whangbo, *Organic Superconductors (Including Fullerenes)*, Prentice Hall, Englewood Cliffs, New Jersey, 1992.
2 É. B. Yagubskii, I. F. Shchegolev, V. N. Laukhin, P. A. Kononovich, M. V. Karatsovnik, A. V. Zvarykina and L. I. Buravov, *Pis'ma Zh. Eksp. Teor. Fiz.*, 1984, **39**, 12.
3 J. M. Williams, H. H. Wang, M. A. Beno, T. J. Emge, L. M. Sowa, P. T. Copps, F. Behroozi, L. N. Hall, K. D. Carlson and G. W. Crabtree, *Inorg. Chem.*, 1984, **23**, 3839.
4 H. H. Wang, M. A. Beno, U. Geiser, M. A. Firestone, K. S. Webb, L. Nuñez, G. W. Crabtree, K. D. Carlson, J. M. Williams, L. J. Azevedo, J. F. Kwak and J. E. Schirber, *Inorg. Chem.*, 1985, **24**, 2465.
5 T. J. Emge, H. H. Wang, P. C. W. Leung, P. R. Rust, J. D. Cook, P. L. Jackson, K. D. Carlson, J. M. Williams, M.-H. Whangbo, E. L. Venturini, J. E. Schirber, L. J. Azevedo and J. R. Ferraro, *J. Am. Chem. Soc.*, 1986, **108**, 695.
6 T. J. Emge, H. H. Wang, M. K. Bowman, C. M. Pipan, K. D. Carlson, M. A. Beno, L. N. Hall, B. A. Anderson, J. M. Williams and H. H. Whangbo, *J. Am. Chem. Soc.*, 1987, **109**, 2016.
7 N. Yoneyama, A. Miyazaki, T. Enoki and G. Saito, *Synth. Met.*, 1997, **86**, 2029.
8 J. M. Williams, A. M. Kini, H. H. Wang, K. D. Carlson, U. Geiser, L. K. Montgomery, G. J. Pyrka, D. M. Watkins, J. M. Kommers, S. J. Boryschuk, A. V. Strieby Crouch, W. K. Kwok, J. E. Schirber, D. L. Overmyer, D. Jung and M.-H. Whangbo, *Inorg. Chem.*, 1990, **29**, 3272.
9 A. M. Kini, U. Geiser, H. H. Wang, K. D. Carlson, J. M. Williams, W. K. Kwok, K. G. Vandervoort, J. E. Thompson, D. L. Stupka, D. Jung and M.-H. Whangbo, *Inorg. Chem.*, 1990, **29**, 2555.
10 U. Geiser, A. J. Schultz, H. H. Wang, D. M. Watkins, D. L. Stupka, J. M. Williams, J. E. Schirber, D. L. Overmyer, D. Jung, J. J. Novoa and M. H. Whangbo, *Physica C*, 1991, **174**, 475.
11 U. Geiser, J. A. Schlueter, H. H. Wang, A. M. Kini, J. M. Williams, P. P. Sche, H. I. Zakowicz, M. L. VanZile, J. D. Dudek, P. G. Nixon, R. W. Winter, G. L. Gard, J. Ren and M.-H. Whangbo, *J. Am. Chem. Soc.*, 1996, **118**, 9996.
12 H. H. Wang, M. L. VanZile, J. A. Schlueter, U. Geiser, A. M. Kini, P. P. Sche, H. J. Koo, M. H. Whangbo, P. G. Nixon, R. W. Winter and G. L. Gard, *J. Phys. Chem. B*, 1999, **103**, 5493.
13 M. Kurmoo, A. W. Graham, P. Day, S. J. Coles, M. B. Hursthouse, J. L. Caulfield, J. Singleton, F. L. Pratt, W. Hayes, L. Ducasse and P. Guionneau, *J. Am. Chem. Soc.*, 1995, **117**, 12209.
14 T. K. Hansen, J. Becher, T. Jorgensen, K. S. Varma, R. Khedekar and M. P. Cava, *Org. Synth.*, 1995, **73**, 270.

15 K. S. Varma, A. Bury, N. J. Harris and A. E. Underhill, *Synthesis*, 1987, 837.
16 R. J. Willenbring, J. Mohtasham, R. Winter and G. L. Gard, *Can. J. Chem.*, 1989, **67**, 2037.
17 G. W. Gokel, D. J. Cram, C. L. Liotta, H. P. Harris and F. L. Cook, in *Organic Synthesis*, ed. C. Johnson, John Wiley & Sons, New York, 1977, Vol. 57, p. 30.
18 T. J. Emge, H. H. Wang, M. A. Beno, J. M. Williams, M. H. Whangbo and M. Evain, *J. Am. Chem. Soc.*, 1986, **108**, 8215.
19 D. A. Stephens, A. E. Rehan, S. J. Compton, R. A. Barkhau and J. M. Williams, *Inorg. Synth.*, 1986, **24**, 135.
20 P. Guionneau, C. J. Kepert, G. Bravic, D. Chasseau, M. R. Truter, M. Kurmoo and P. Day, *Synth. Met.*, 1997, **86**, 1973–1974.
21 H. H. Wang, J. R. Ferraro, J. M. Williams, U. Geiser and J. A. Schlueter, *J. Chem. Soc., Chem. Commun.*, 1994, 1893.
22 J. E. Eldridge, C. C. Homes, J. M. Williams, A. M. Kini and H. H. Wang, *Spectrochim. Acta*, 1995, **51A**, 947.
23 J. Dong, J. L. Musfeldt, J. A. Schlueter, J. M. Williams, P. G. Nixon, R. W. Winter and G. L. Gard, *Phys. Rev. B*, 1999, **60**, 4342.
24 I. Olejniczak, B. Jones, Z. Zhu, J. Dong, J. L. Musfeldt, J. A. Schlueter, E. Morales, U. Geiser, P. G. Nixon, R. W. Winter and G. L. Gard, *Chem. Mater.*, 1999, **11**, 3160.
25 H. J. Koo, M. H. Whangbo, J. Dong, I. Olejniczak, J. L. Musfeldt, J. A. Schlueter and U. Geiser, *Solid State Commun.*, 1999, **112**, 403.
26 H. H. Whangbo and R. Hoffmann, *J. Am. Chem. Soc.*, 1978, **100**, 6093.
27 J. Ren, W. Liang and M. H. Whangbo, *Crystal and Electronic Structure Analysis Using CAESAR*, 1998, PrimeColor Software, Inc. (this book can be downloaded free of charge from the website: http://www.PrimeC.com/).
28 D. Beckmann, S. Wanka, J. Wosnitza, J. A. Schlueter, J. M. Williams, P. G. Nixon, R. W. Winter, G. L. Gard, J. Ren and M.-H. Whangbo, *Eur. Phys. J. B*, 1998, **1**, 295.
29 M.-H. Whangbo, J. M. Williams, P. C. W. Leung, M. A. Beno, T. J. Emge and H. H. Wang, *Inorg. Chem.*, 1985, **24**, 3500.